Design, Simulation and Testing of the OOK NRZ Modulation Format for Free Space Optic Communication in a Simulation Box

Ales VANDERKA, Lukas HAJEK, Jan LATAL, Jan VITASEK, Petr KOUDELKA

Department of Telecommunications, Faculty of Electrical Engineering, VSB–Technical University of Ostrava, 17.listopadu 15/2172, 708 33 Ostrava-Poruba, Czech Republic

ales.vanderka@vsb.cz, lukas.hajek@vsb.cz, jan.latal@vsb.cz, jan.vitasek@vsb.cz, petr.koudelka@vsb.cz

Abstract. *This article deals with the construction of a modulator and demodulator for Free-Space Optical (FSO) communication. In FSO optics, the modulated optical signal is propagated in the constantly changing environment (atmosphere). The optical signal is strongly influenced by the actual composition of air, which is directly linked to the change in refractive index in the turbulent cells. This article examines primarily the appropriate modulation format for FSO. For this purpose, one type of an OOK-NRZ modulator and one type of a demodulator were designed. This article also describes the construction of two types of photo detectors (the high impedance and the transimpedance ones). All electronic constructions were tested in the Micro-Cap simulator and they were experimentally measured as well. For the OOK NRZ modulation the, maximum transmission speed achieved the value of 160 Mbps. Measuring the quality of the modulation formats was carried out under mechanical and thermal turbulences. The last part of this work gives the results of the measurements of fog influences.*

Keywords

Construction, demodulator, Free Space Optic, lasers, modulation, NRZ, photodetectors.

1. Introduction

At FSO the communication runs by means of light in the atmosphere under the full-duplex operation. There is a carrier wave that is used for communication. This wave includes one or more wave divisible channels. The power of these channels is transmitted by one or more volumes. The FSO transmission path consists of two optical heads integrating both the optical transmitter and the receiver. The transmitting unit is composed of a modulator and radiation sources. The receiver section consists of a detector and a demodulator. Both the receiver and the transmitter are equipped with adaptive optics. Adaptive optics focuses the optical beam on the detector and this way it increases its profits. In the optical transmitter, the laser, laser diodes (LDs), LEDs, or infrared emitting diodes (IREDs) are used as the sources of radiation. The sources of radiation are modulated either indirectly or directly by changing the excitation current of the optical source. The communication takes place in the transmission windows of 850 nm, 1550 nm, and at longer wavelengths. At the receiver, the photodiodes of the PIN type as well as more sensitive avalanche photodiodes APD are used [1], [11].

The advantages of FSO are the installation speed, operating in an unlicensed band, security (complex interception), high data rate and ease of portability. FSO can be used for the last mile networks as a replacement for the RF [1], [2].

As compared with the RF system, FSO is less affected by rain and snow, but, on the other hand, it can be more affected by atmospheric turbulences and fog. The RF communication is very sensitive to rainfall (hydrometeorits). During the turbulences, the turbulent cells of different refractive indices are created. These refractive indices vary due to the fluctuations of their density and temperature. These changes in refractive index bend the light beam (from its original path), resulting in fluctuations of the received light output. The size and frequency of the fluctuations of the received power depend on the amplitude of the turbulent cells. The change of path occurs when the beam passes through a cell that is bigger than this volume. When the beam passes through the smaller cell, there appears the deformation of the wave front [18].

The aerosol particles (mist) strongly influence the light beam. The light beam is mostly absorbed by the

fog particles of the size equal to the wavelength of the light source. This leads to a long-term loss of the power in a matter of hours [3], [4], [5], [6]. The attenuation of the atmosphere ranges from 0.22 dB·km^{-1} (visibility of 20 km) for clean environment to 271 dB·km^{-1} (visibility of $0 - 50$ m) for dense mist and it is therefore necessary to deploy the hybrid FSO/RF [3], [10].

FSO uses LEDs and laser sources with the wavelengths corresponding to an atmospheric transmission window (with the minimum attenuation) [19].

An important parameter for the FSO links is the used modulation format, which can increase its reliability. At FSO, the On-Off Keying modulation (OOK) is used most often. It is used in the NRZ and RZ variants. The OOK is used because of its good spectral efficiency and easy circumferential solutions [6], [7], [8], [9], [10], [11].

The optimal limit level of FSO is affected by the turbulence and absorption of the atmosphere. To stop this negative effect, it is necessary to apply some adaptive decision limit levels. This necessity increased the interest in transition to other types of the modulation formats. These may be the SIM modulation formats (Subcarrier Intensity Modulation). In the SIM modulation format, the modulations BPSK, QPSK, and others modulations. The solution of the adaptive decision levels in the SIM modulation formats is not necessary any longer [2], [12], [13], [14], [15], [16], [17].

The atmospheric influence affects the modulated optical beam and it leads to incorrect detection of the received signal. This is the reason why at present the modulation formats that would be resistant to these interfering influences were searched for. Concerning the modulation formats, it is necessary to find a compromise between the photo-efficiency, bandwidth, and sensitivity to interference, cost and demands of the manufacture [2, 13].

In the first chapter of this article, the authors focus on the observations of the influences of the atmospheric phenomena on the FSO modulation formats. In the second chapter the theory of the used modulations formats including their mathematical descriptions is given. In the third chapter the principles of modulation of laser diodes are described. This chapter also contains the principles of a detection process of the optical signal with the basic circuit diagram of photodiodes. The fourth chapter describes the design of the circuits and their testing kits for the modulation formats OOK-NRZ and BPSK. In the fifth chapter the description of the measuring station and the techniques for measuring the impact of the atmospheric phenomena on an eye diagram is given. In the sixth chapter the data taken from the eye diagram of the OOK-NRZ modulation are analyzed. Finally, the last chapter is devoted to the simulation in the OptiSystem environment. The simulation gives an account of the influence of the structural parameter of the refraction index C_n^2 on the OOK-NRZ modulation format.

2. Modulation of Optical Signal

A modulation technique influences parameters, such as bandwidth and energy efficiency, which affect the total system power. The most frequently used modulation for free space optics is OOK (On-Off Keying). The other modulation formats are PSK (Phase Shift Keying), DPSK (Differential Phase Shift Keying) and orthogonal modulation formats. The choice of the modulation technique depends on the type of use, where the compromise between the complexity, optical power, photo efficiency and bandwidth is important. An electrically modulated signal is converted into an optical signal in an E/O converter. The most frequently used modulation type is the intensity modulation when the immediate power of the transmitted energy with the required wavelength is modulated. A photo-detector converts an optical signal into an electrical signal on the site of a receiver. Finally, the information is obtained from the electrical signal by demodulation [14].

The modulation formats exhibit different sensitivity on the turbulence flow in the transmission environment (atmosphere), which causes decrease in received optical power. The level of the received optical power is significant for maintaining the correct bit-error-ratio (BER) with the same bit-rate. The modulation formats should be energetically efficient with low difficulty on the construction of both the receiver and the transmitter. They should also have the smallest bandwidth [2].

The main reason for using the OOK modulation is its simplicity of implementation, but its fixed limit (threshold) level is not optimal because of the fluctuations in the received power. In the PPM (Pulse Position Modulation) the threshold level is not used. There is increased photo-efficiency to the detriment of the complexity of implementation (the need for synchronization) and the bandwidth [13], [31].

The Subcarrier Index Modulation (SIM) does not also use the threshold level and does not require such a wide bandwidth as the PPM modulation, but it has smaller photo-efficiency [13], [31].

3. On-Off Keying Modulation

It is a type of the intensity modulation belonging to the ASK modulation, in which binary information is

represented by the presence or absence of an optical signal. The decision level compensates the probability of the error log 0 and log 1 and is dependent on the received power and noise. This type of modulation is most widely used in free space optics. The production of the transmitter and the receiver is simple. It is resistant to nonlinearity on the laser and the external modulator. The OOK is more sensitive to atmospheric turbulences and other disturbing influences when the fluctuations of the received level occur. At the error rate of BER 10^{-9} the photo-efficiency of this modulation is PPB = 39 dB [2], [16], [20], [25]. The rate of errors for this modulation is defined as follows [24], [26], [27], [31]:

$$\mathrm{BER}_{\mathrm{OOK\text{-}NRZ}} = \frac{1}{2}\mathrm{erfc}\left(\frac{1}{2\sqrt{2}}\sqrt{\mathrm{SNR}}\right). \qquad (1)$$

4. Laser Diode Driver

In our tests the generator Stanford CG635 was used as the source of the pseudo random sequences. From the generator the signal entered the modulator, in which the LVDS signal was converted into a modulation signal for the laser diode (Tab. 1). The laser diode was placed in a temperature and current stabilized cube (TCLDM9) from the Thorlabs Company. The Thorlabs thermal stabilizer of the type designation TED200C as well as the LDC205C current stabilizer were also used.

The light signal emitted from a laser diode was collimated to the photo-detector (for 850 nm - A220TM-B and 1550 nm - C230TME-C) using a collimator. The laser beam went through the simulation box, in which it was influenced by the atmospheric effects (the wind turbulence, temperature turbulence and fog). The influenced modulated laser beam fell on the photo-detector, in which it was converted back to an electrical signal and afterwards demodulated. On the receiving side there were eye diagrams, which were using an oscilloscope (LeCroy 204Xi). The parameters of the eye diagrams deteriorated due to the atmospheric environment.

The laser diode is modulated by using the input TCMLD9, which is driven by a temperature and current controller. The RF input is directly connected to the laser diode through a bias-tee (Fig. 1). In the test the bias-tee was designed to bring the DC current and at the same time to bring the modulation signal to the laser diode. The RF input had an SMA connector with the termination of 50 Ω. To this connector an AC component with the frequency of 500 MHz can be brought.

Tab. 1: The parameters of used laser and photo-detector diode.

Laser diode L850P010	
Threshold current	25 mA
Operating current	50 mA
Wavelength	850 nm
Optical power	10 mW
Laser diode ML925B45F	
Threshold current	10 mA
Operating current	30 mA
Wavelength	1550 nm
Optical power	5 mW
Photo-detector Thorlabs PDA 10A-EC	
Spectral sensitivity	200–1100 nm
Active area	0.8 mm^2
Bandwidth	150 MHz
Photo-detector sensitivity (850 nm)	0.35 A/W
Photo-detector Thorlabs PDA 10CF-EC	
Spectral sensitivity	700–1800 nm
Active area	0.2 mm^2
Bandwidth	150 MHz
Photo-detector sensitivity (1550 nm)	0.95 A/W

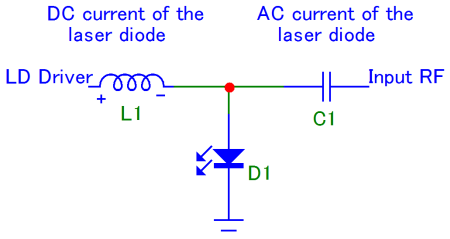

Fig. 1: Internal wiring of the driver for modulation LD L850P010 in the MicroCap software.

The modulation voltage necessary for achievement of the desired modulation current can be derived by the following formula, in which $R_{vst} = 50\ \Omega$:

$$U_{RF} = I_{MOD} \cdot R_{vst}\,[V; A, \Omega]\,. \qquad (2)$$

For the modulation of the laser diodes the changes of the driving current are used (Fig. 2). This current consists of a DC and an AC component. The DC component keeps the laser diode in the operation mode, in which its characteristic is linear (exceeding I_{th}). The principle of the modulation when the laser diode is modulated by the OOK signal is shown in (Fig. 2).

5. OOK Modulator

The square signal with the voltage amplitude peak-to-peak U_{pp} = 0.5 V emits from the generator PRBS, since it is necessary to change the voltage of the modulation signal according to the type of the used laser diode. The OOK modulator is placed behind the gen-

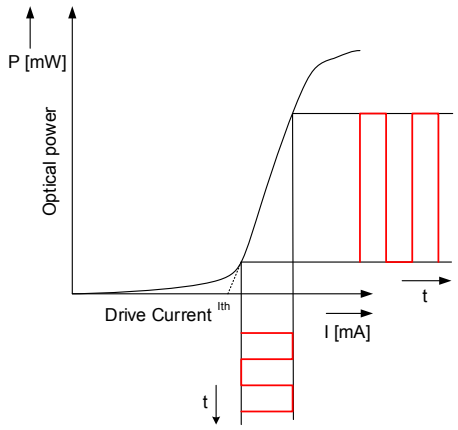

Fig. 2: P-I laser diode characteristic and its modulation [22].

erator PRBS consisting of a voltage divider and the operational amplifier LM7171 (Fig. 3). The LM7171 allows the current of the output strain up to 100 mA because the signal from the modulator is connected directly to the laser diode through a Bias-tee.

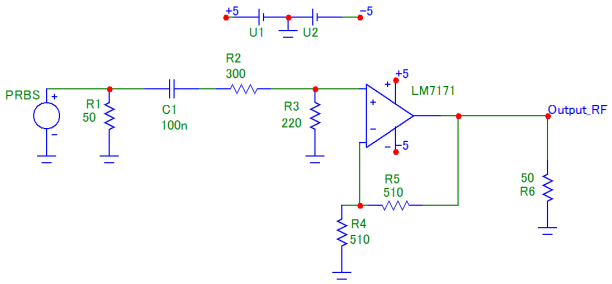

Fig. 3: Diagram of wiring the OOK modulator in the simulation in MicroCap.

The frequency characteristic was simulated in program MicroCap 11. The decrease of the amplitude by 3 dB occurred at $f_{-3dB} = 160$ MHz (Fig. 4) [26].

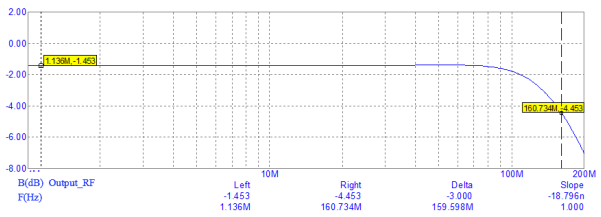

Fig. 4: Diagram of wiring the OOK modulator in the simulation in MicroCap.

The measured eye diagram from the output of the assembled OOK-NRZ modulator is illustrated in (Fig. 5).

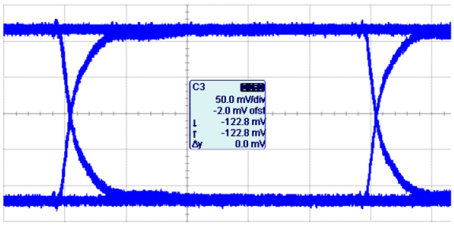

Fig. 5: Diagram of wiring the OOK modulator in the simulation in MicroCap.

6. Electronic Design of Photo-detector and Demodulator OOK

For the electronic design of a photo-detector in the MicroCap, the transimpedance connection of a photodiode with the low-noise operational amplifier OPA847 of a large bandwidth was used (Fig. 6). The amplifier OPA847 is optimized for this circuit. It has the largest bandwidth with the lowest input noise and with the largest slew rate. As for the electronic design, the operational amplifier OPA846 was chosen for the subsequent amplification [28], [29].

The photodiode Thorlabs FDS010 was used. It is spectral sensitivity was from 200 nm to 1100 nm, the minimum bandwidth was 350 MHz and the capacity was from 2 pF (depending on the supplying voltage).

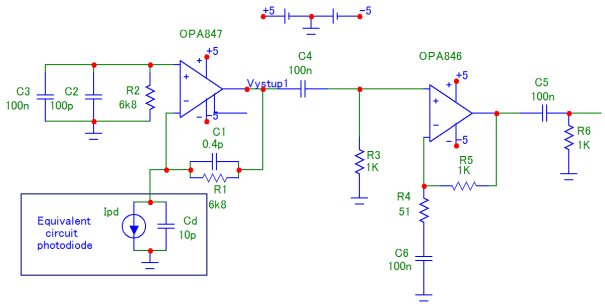

Fig. 6: The diagram of photo-detector connection with the equivalent circuit of a photodiode.

At the maximal amplitude of the light signal, the total amount of the optical power falling on the photodetector is 0.166 mW. It results from the characteristic of the photodiode sensitivity (Fig. 7) that the current of 0.0662 mA (at $\lambda = 650$ nm) flew through this photodiode. In order to maintain the greatest bandwidth and to increase the signal sufficiently, the bandwidth was calculated (see Eq. (3)). The bandwidth of 95 MHz and the output voltage of 0.45 V were selected at the current of the photodiode of 0.0662 mA. It was also counted on the capacity of the photodiode of 10 pF, with the involvement of the reverse voltage of -5 V, to which the capacitance between the differential inputs

as well as the input capacitance of the operational amplifier (2.5+1.2) pF was added.

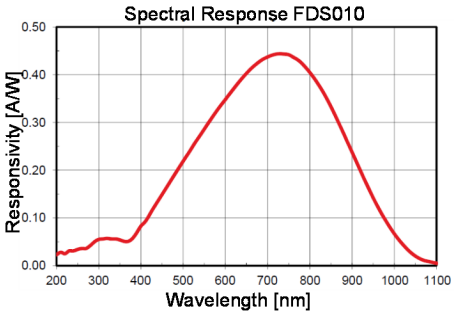

Fig. 7: Relative spectral sensitivity dependent on wavelength for photodiode FDS 010.

To stabilize the circuit and to avoid the peak amplification of certain frequencies (oscillation), the photodiodes capacity had to be compensated by the parallel capacity C_1 at the resistance R_1 (see Eq. (4)) .

$$f_{-3\mathrm{dB}} = \sqrt{\frac{GBP}{2\pi \cdot R_1 \cdot C_D}} = \\ = \sqrt{\frac{3900 \cdot 10^6}{2\pi\ 6.8 \cdot 10^3\ 10 \cdot 10^{-12}}} = 95\ \mathrm{MHz}. \tag{3}$$

$$R_1 = \frac{GBP}{2\pi \cdot (f_{-3dB})^2 \cdot C_D} \\ = \frac{3900 \cdot 10^6}{2\pi\ (95.5 \cdot 10^6)^2 \cdot 10^{-12}} = 6.8\ \mathrm{k\Omega}. \tag{4}$$

To stabilize the circuit and to avoid the peak amplification of certain frequencies (oscillation), the photodiodes capacity had to be compensated by the parallel capacity C_1 at the resistance R_1 (see Eq. (4)).

$$\frac{1}{2\pi \cdot R_1 \cdot C_1} = \sqrt{\frac{GBP}{4\pi \cdot R_1 \cdot C_D}} \\ C_1 = \frac{1}{2\pi\ 6800 \sqrt{\frac{3900 \cdot 10^6}{4\pi \cdot 6800 \cdot 14 \cdot 10^{-12}}}} = 0.409\ \mathrm{pF}. \tag{5}$$

The capacity of the photodiode is compensated by the capacity C_1. The capacity C_1 is estimated by using Eq. (5). The SMD resistance already includes the parasitic capacitance of about 0.2 pF, therefore the capacity of 0.2 pF was only added to the resistance. It was verified in the simulation. To determine the optimum value of the compensating capacity the temporal analysis was done. It was a temporal analysis of the transimpedance amplifier circuit done by the input square signal from the photodiode with the frequency of 20 MHz and the current $I_{ss} = 66.2$ µA. During the simulation the compensatory capacity C_1 was changed (Fig. 8), where particular colours of the waveforms correspond to these values (0.2 pF – red, 0.3 pF – green, 0.4 pF – blue, and 0.5 pF – purple). The optimal value of the compensating capacity was between 0.3 and 0.4 pF. When small capacity was selected, the circuit was unstable and it began to oscillate. On the contrary, when a larger capacity was responsible for, the optimal capacity led to the deformation of the output signal and to the decrease of the bandwidth of this connection.

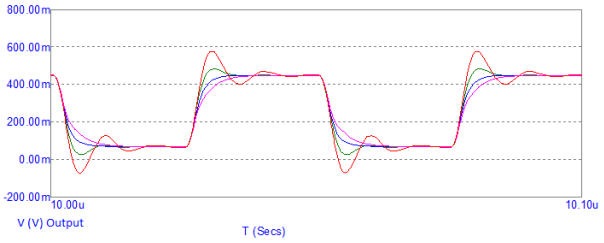

Fig. 8: The signal from transimpedance amplifier at the change of compensating capacity at frequency of square signal of 10 MHz in MicroCap.

To minimize the output noise, the following electronic components were added between the non-inverting input and ground: the resistance value of R_2 = 6K8 and the capacity of the values of C_2 = 100 pF and C_3 = 100 nF. Resistor R_4 was connected to the ground through capacitor C_6, so the amplification of the non-inverting amplifier was A=1 for the prospective DC component and the required gain for the AC component. Thanks to this, the bottom cut-off frequency of the amplifier was $f_{-3\mathrm{dB}} = 31$ kHz.

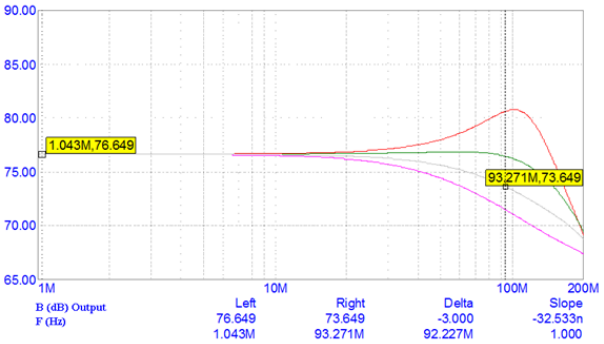

Fig. 9: Frequency characteristic of transimpedance connection in MicroCap.

Subsequently, the frequency characteristic of the transimpedance connection was depicted in the simulation. The frequency of the input signal was changed in the range of 1 MHz to 100 MHz. The output voltage was measured in decibels when the value decreased by 3 dB at $f_{-3\mathrm{dB}} = 93.2$ MHz (Fig. 9).

7. Measuring Station for Testing Atmospheric Effects on the Modulations Formats at FSO

For the purposes of the measurements, a measuring station was established (Fig. 10). It consists of a measuring box, the length of which is 2.5 m. It is equipped with powerful fans to enable measuring of the influence of the mechanical turbulences on the optical beam. For the simulation of the thermal turbulences the direct heaters were used and the glycerin mist generator (Antari F-80Z) was used in order to create the fog. The box was placed on an iron construction, ahead it the holder of a laser diode was installed on an aluminium construction. The laser diode shone upright through the faces of the box, the light beam landed on the photo-detector. The photo-detector was also placed on the aluminium construction.

To provide the temperature and current stabilization of the laser diode, the Thorlabs equipment was used (TDC205C – setting of the DC component of the current, TED200C – setting of the operating temperature, TLCLDM9 – the holder of the laser diode with the input for the modulation voltage). To generate the signal PRBS (pseudo-random bit sequences), the Stanford CG635 generator was used, the output of which was connected to the modulator where it was possible to change the amplitude of the modulation voltage for a certain laser diode. This signal directly modulates the laser diode installed in the TLLDM9 holder. The laser beam from the laser diode was collimated and focused on the photo-detector where the optical signal was converted back to the electrical signal. The signal from the photo-detector was observed directly using an eye diagram on an oscilloscope (in case of the OOK modulation). In case of BPSK modulation the signal was observed at the output of the demodulator only. The measurement was performed with a constructed transimpedance photo-detector and also with Thorlabs detectors (PDA 10C and PDA 10A–EC), the bandwidth of which is larger.

At measuring, the same attenuations were ensured by the effect of the box walls when during each measuring the optical beam passed through one Plexiglas wall. The second wall was either withdrawn, or the passage was created through it, so the further decay was impossible.

For the measurements, the photodetector by Thorlabs PDA10A for the wavelength of 850 nm and photodetector PDA 10CF–EC for the wavelength of 1550 nm were used. Because of using another photodetector and also due to difficult collimation of the optical beam, the parameters were not equal. It is therefore impossible to compare the results gained from measuring with the wavelength of 1550 nm.

8. Thermal Turbulences

During measurements the thermal turbulences the bottom wall of the box was removed as well as the wall ahead the detector. Hot air was blown into the box using direct heaters (CTH–5000 Empire), which were placed under the box. The output of the heaters was 2kW/piece, the temperature of the generated hot air was 48 °C and the flow rate reached 3.5 m·s^{-1}. The heated air was sucked by, a ventilator, which was placed on the top of the lid. The warm air could also freely issue fromthe open side. The measurement was carried out with several combinations of theswitched fans. Because of the reference, the eye diagram was always measured at the inactive hot-air fans. Then the hot-air fans were gradually switched on in the following combinations: the 1st and 3rd fan switched on, the 1st, 2nd and 3rd fan switched on. It is shown in (Fig. 11). In (Fig. 14, Fig. 15, Fig. 16) there are eye diagrams for the OOK–NRZ modulation at the transmission speed of 20 Mb·s^{-1}.

The fan at the top of the box remained active even at the thermal turbulences due to the extraction of the excessive hot air to prevent the box from being filled up with the air of the same temperature. The temperature in the box with the three fans on was measured using

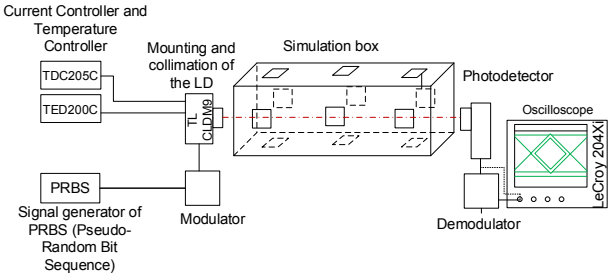

Fig. 10: The diagram of station connection.

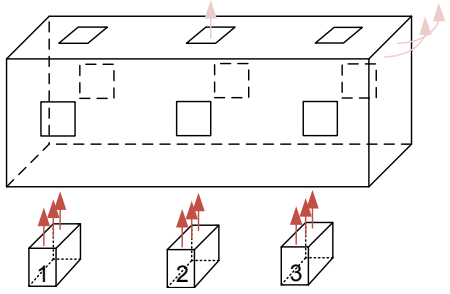

Fig. 11: Box for thermal turbulences.

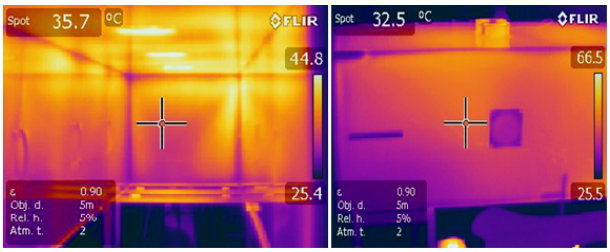

Fig. 12: Temperature distribution in the box when the three direct heaters are switched on.

a thermal camera (FLIR E50).Alternating of the areas with warm and cold air can be seen in Fig. 12).

9. Measuring Eye Diagram

For the detailed evaluation of the measurement the double value of the reserve signal–to–noise was deducted from the eye diagram (Fig. 13) from the LeCroy oscilloscope). Before each measurement of the atmospheric effects, the reference value of the eye diagram was recorded. Afterwards, the eye diagram was measured with the atmospheric influences. Then the ratio between the reference of the eye diagram opening and the value of the opening of the eye diagram under the influences of the atmosphere was calculated. This ratio was brought to the graph.

$$A = \frac{A_{ref}}{A_{inf}} \; [-], \tag{6}$$

Where the variable A_{ref} represents the variable reference eye diagram and the A_{inf} represents the variable eye diagram with atmospherical influence.

The optical beam was influenced significantly by the thermal turbulences; there was significant fluctuation in the received optical power. This caused the closure of the eye diagram. With each added thermal fan the size of the turbulences increased. These thermal turbulences caused increasing of the closure of the eye diagram. The worst values were achieved for significant difference intemperature when the 1st and 3rd thermal fans were switched on. Thus, two areas with the thermal turbulences were formed and in the middle there was airflow of the room temperature.

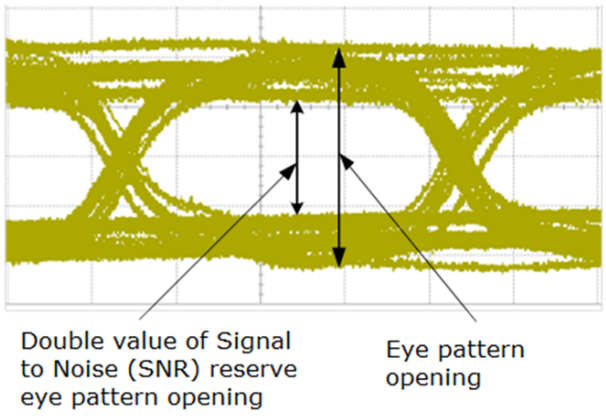

Fig. 13: Measuring of eye diagram opening.

Figure 14 shows the eye diagram without any atmospheric turbulences. Figure 15 shows the eye diagram when the 1st and 3rd thermal fans were switched on. In this case the atmospheric turbulences have significant influence on the fluctuation of the eye diagram. Figure 16 shows the worst state of the eye diagram when all thermal fans were switched on.

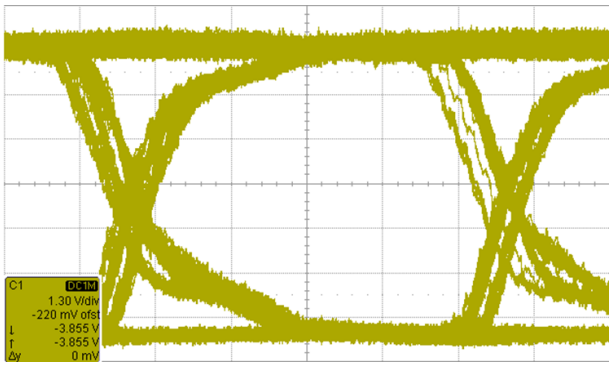

Fig. 14: The eye diagram (OOK–NRZ modulation – 20 Mb·s^{-1}) for switched 1st direct heater.

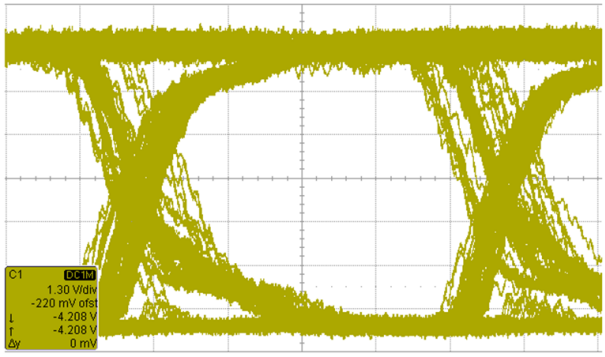

Fig. 15: The eye diagram (OOK–NRZ modulation – 20 Mb·s^{-1}) for switched 1st and 3rd direct heater.

In Fig. 17, there is the dimension of the turbulences depending on the data rate. It can be seen that as the thermal turbulences grow, the discharge of the optical power grows too. At the wavelength of 1550 nm was significantly influenced by the thermal turbulences (Fig. 18), but it did not depend on the size of the turbulences so much as it did at the wavelength of 850 nm. With increasing size of the turbulences, there was not such a significant decrease of the received power. The wavelength of 1550 nm the beam was too collimated on the surface of the photo-detector. This surface was much smaller than at the 1stThorlabsphoto-detector and at the deflection of the beam due to the turbulences there was bigger power leakage.These thermal

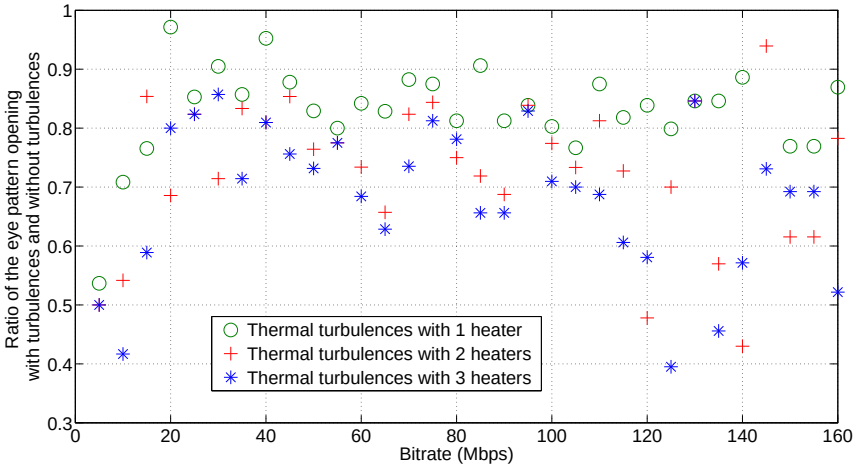

Fig. 17: Measuring of the influence of turbulences on the optical beam with used OOK–NRZ modulation $\lambda = 850$ nm.

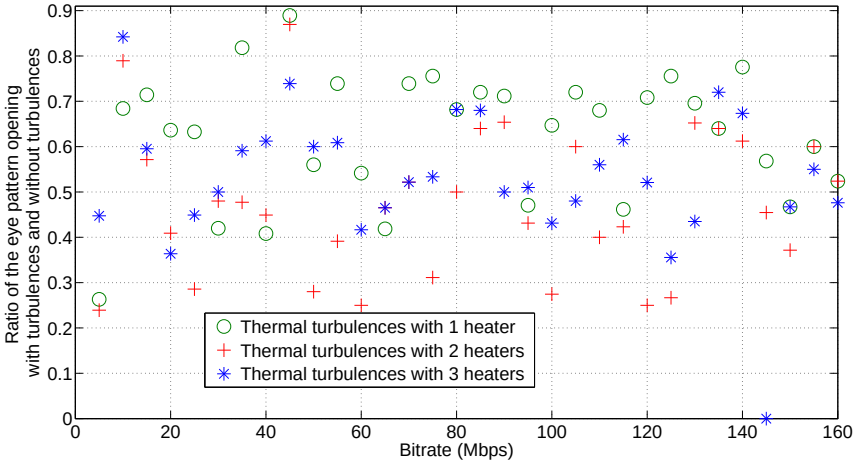

Fig. 18: Measuring of the influence of turbulences on the optical beam with used OOK–NRZ modulation $\lambda = 1550$ nm.

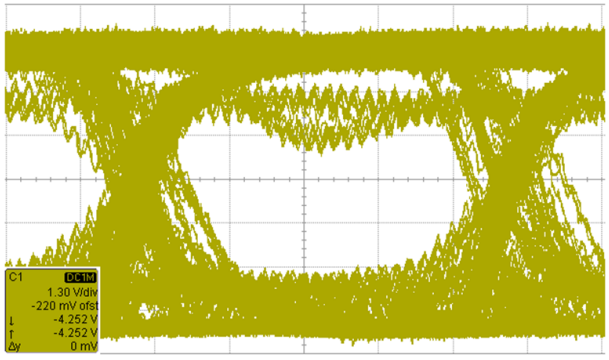

Fig. 16: The eye diagram (OOK–NRZ modulation – 20 Mb·s^{-1})for switched 1st, 2nd, 3rd direct heater.

turbulences manifest themselves mainly during clear weather when the surface of the ground is heated and the warm air convects. The problem may occur when the head is installed over the roof of the building heated by the sun, and the warm air interferes with the optical path. For these reasons, it is necessary to have a sufficient diameter of the optical beam on the receiver and also to plan for a sufficient power reserve.

10. Simulation of Thermal Turbulences in the OptiSystem Environment for OOK–NRZ Modulation

The simulation in the OptiSystem environment was set according to the parameters of the real measurements with a photodiode transimpedance wiring. For the modulation of the optical radiation the direct modulation was not used. The Mach-Zehnder modulator was used instead. The wiring of the OOK-NRZ modu-

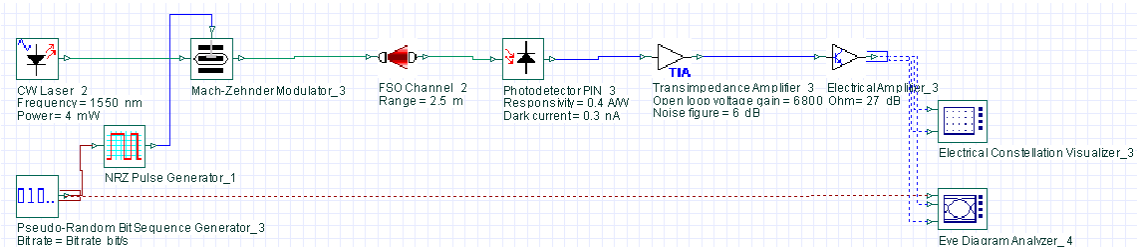

Fig. 19: The wiring scheme of Free Space Optical link with OOK–NRZ modulation.

lation consisted of a laser diode with the optical power of 4 mW. It was followed by the Mach-Zehnder modulator. To this modulator the output from the OOK-NRZ modulator was connected. The OOK-NRZ modulator was driven by a signal from the generator of pseudo-random sequences. Then the modulated optical signal passed through the simulator of the atmospheric environment (FSO Channel), where the averages of the optical transmitter and receiver were set as well as the atmospheric attenuation. For the measurements of the turbulences the structure parameter of the refractive index C_n^2 was set. The optical signal fell on the photodetector PIN. The following values were set: the gain of the operational amplifier (using resistance), sensitivity of the photodiode and the noise parameters. The signal was then amplified by an operational amplifier with the gain of 27 dB. The amplified signal was transferred to the analyzer of the eye diagram where the size of the eye opening was deducted. The scheme of wiring for the OOK-NRZ modulation in the OptiSystem is shown in Fig. 19.

In Tab. 2 the set parameters of the optical free space link are described. These parameters were set in the simulation according to the real measurements.

In Fig. 20, Fig. 23, Fig. 24 there are eye diagrams for the OOK-NRZ modulation for the bit rate of 20 Mb·s^{-1}. The eye diagrams without any structural parameters of the refractive index and with the structural parameters of the refractive index $C_n^2 =$

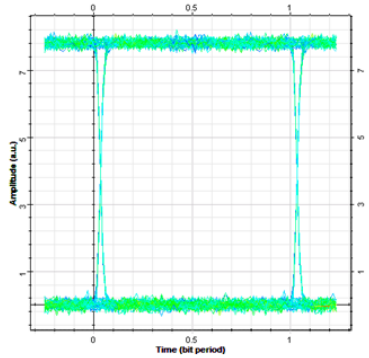

Fig. 20: Comparison of eye diagrams for OOK-NRZ modulation with structural parameters of refractive index $C_n^2 = 6.2 \cdot 10^{-10}$ m$^{-2/3}$.

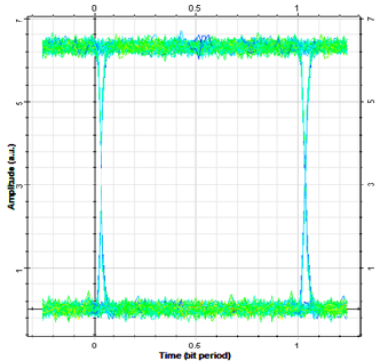

Fig. 21: Comparison of eye diagrams for OOK-NRZ modulation with structural parameters of refractive index $C_n^2 = 8.5 \cdot 10^{-10}$ m$^{-2/3}$.

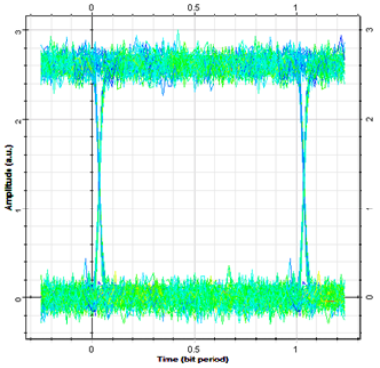

Fig. 22: Comparison of eye diagrams for OOK-NRZ modulation with structural parameters of refractive index $C_n^2 = 8 \cdot 10^{-10}$ m$^{-2/3}$.

$6.2{\cdot}10^{-10}$ [m$^{-2/3}$] (Fig. 20), $8.5{\cdot}10^{-9}$ [m$^{-2/3}$] (Fig. 21), $8 \cdot 10^{-6}$ [m$^{-2/3}$] (Fig. 22) were observed. It can be seen from these eye diagrams that with the increasing structural parameters of the refractive index (the increasing turbulences) the noise of the received signal (closing of the eye diagram) increased as well. The eye diagrams of the simulations in the OptiSystem are processed into graphs. In the graphs the data are represented by the quotient of opening of the measured eye diagram with and without the activated structural parameter of the refractive index $C_n^2 = 6.2{\cdot}10^{-10}$ [m$^{-2/3}$]; $8.5 \cdot 10^{-9}$ [m$^{-2/3}$]; $8 \cdot 10^{-6}$ [m$^{-2/3}$]. The diagram (Fig. 23): at $\lambda = 1550$ nm) shows the influence of the turbulence size depending on the bit rate where

Tab. 2: Set parameters for simulation in OptiSystem environment.

Parameter	Value
Optical power	4 mW
Wavelengths	850 and 1550 nm
Diameter of photo-detector	0.6 mm
Diameter of the optical beam on the photo-detector	3.4 mm
Diameter of the optical beam on the photo-detector	3.4 mm
Parameter of turbulence C_n^2	$10^{-18} - 8 \cdot 10^{-6}$ m$^{2/3}$
Amplification of transimpedance amplifier (resistance)	6800 Ω
Dark current	0.3 nA
Sensitivity of photodiode	0.4 A/W
Thermal noise	$18 \cdot 10^{-12}$ A/Hz$^{0.5}$
Following amplification	27 dB

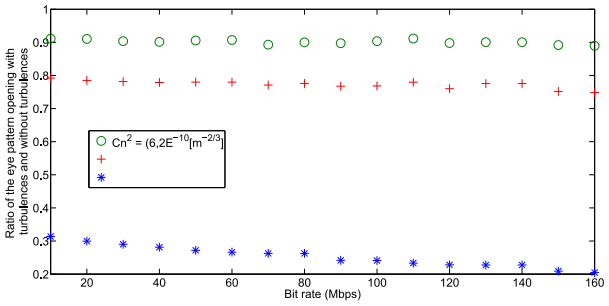

Fig. 23: Measuring of the influence of turbulences on the optical beam using OOK-NRZ modulation and $\lambda = 850$ nm.

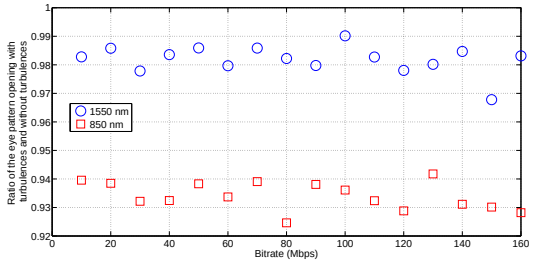

Fig. 24: The effect of the structural parameter of refractive index $C_n^2 = 6.2 \cdot 10^{-10}$ [m$^{-2/3}$] on wavelengths of 1550 nm and 850 nm.

the increase of the thermal turbulences causes the increase of the optical power leakage. This increase is also associated with the transmission speed when the reference value of the opening eye diagram decreases concurrently with the increasing transmission speed, which intensifies the influence of the turbulences. In the OptiSystem simulation, the effects of the turbulences on the eye diagram were similar for both wavelengths, but the wavelength of 1550 nm was less affected by the structural parameter of the refractive index $C_n^2 = 6.2 \cdot 10^{-10}$ [m$^{-2/3}$] (Fig. 24). The effect on both wavelengths equalized together with the increase of the structural parameter of the refractive

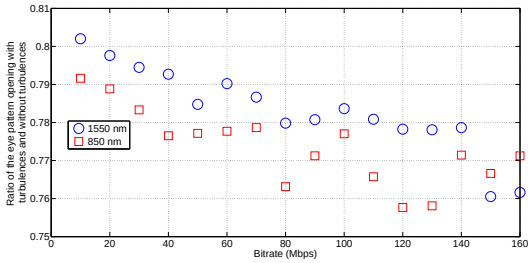

Fig. 25: The effect of the structural parameter of the refractive index $C_n^2 = 8.5 \cdot 10^{-10}$ [m$^{-2/3}$] on the wavelengths of 1550 nm and 850 nm.

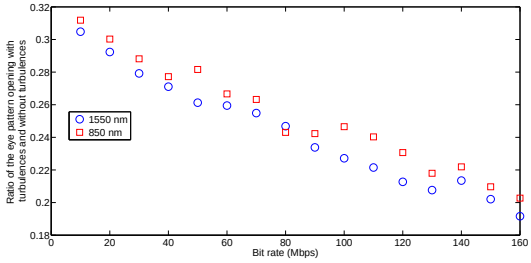

Fig. 26: The effect of the structural parameter of the refractive index $C_n^2 = 8 \cdot 10^{-6}$ [m$^{-2/3}$] on the wavelengths of 1550 nm and 850 nm.

index (Fig. 25). At $C_n^2 = 8 \cdot 10^{-6}$ [m$^{-2/3}$] (Fig. 26) the wavelength of 1550 nm was more affected.

By comparison of real measurements and simulations. The similar behavior is observed in properties of eye diagram dependent on intensity of turbulence. When the turbulence intensity increase the eye diagram reduces and it leads to degradation of BER parameter. This behavior results in degradation of transmission capability of Free Space Optical link. This behavior is more evident in the case of simulations (OptiSystem), than in the case of real measurements.

11. Conclusion

During the measurement of the impact of the turbulent flow on the optical beam, no significant effect of the mechanical turbulences on the received optical power was observed. However, regarding the thermal turbulences, the fluctuation of the received power at the receiver was considerable. This fact is proven by the measured values of the eye diagrams for different types of the modulation and bit rate. The fluctuations of the received optical power caused the decrease in opening the eye diagram. At increasing the turbulence size the closure of the eye diagram was more significant. The most significant closure of the eye diagram occurred at a big temperature difference when the area with the air flow of the room temperature was located in the box

between two areas with temperature turbulences. The bit rate also affects the closure of the eye diagram and the increasing transmission rate leads to the closure of the eye diagram. The closure causes the increase of the BER. The thermal turbulences are mainly manifested in clear weather when the surface of the land is heated and the warm air rises. The problem may occur at installing the head over the roof heated by the sun and the warm air influencing the optical path. For these reasons, it is necessary to provide a sufficient diameter of the optical beam on the receiver as well as to count with a sufficient power reserve.

Acknowledgment

The research described in this article could be carried out thanks to the active support of the Ministry of Education of the Czech Republic within the projects no. SP2014/77, SP2014/147 and SP2015/182. This article was supported by projects Technology Agency of the Czech Republic TA03020439 and TA04021263. The research has been partially supported by the project no. CZ.1.07/2.3.00/20.0217 (The Development of Excellence of the Telecommunication Research Team in Relation to International Cooperation) within the frame of the operation programme Education for Competitiveness financed by the European Structural Funds and from the state budget of the Czech Republic.

References

[1] FRANZ, J. H. and J. V. KUMAR. *Optical Communications Components and Systems*. 1st ed. New Delhi: Narosa Publishing House, 2000. ISBN 978-0849309359.

[2] MAJUMDAR, A. K. and J. C. RICKLIN. *Free-Space Laser Communications: Principles and Advances*. 1st ed. New York: Springer, 2008. ISBN 9780387286778.

[3] WILLEBRAND, H. and B. S. GHUMAN. *Free-Space Optics: Enabling Optical Connectivity in Today's Networks*. Indianapolis: Sams, 2002. ISBN 06-723-2248-X.

[4] KIM, I. I. and J. C. RICKLIN. Wireless optical transmission of fast ethernet, FDDI, ATM, and ESCON protocol data using the TerraLink laser communication system. *Optical Engineering*. 1998, vol. 37, iss. 12, pp. 3143–3155. ISSN 0091-3286. DOI: 10.1117/1.601981.

[5] POPOOLA, W. O. *Subcarrier Intensity Modulated Free-Space Optical Communication Systems*. Newcastle, 2009. Dissertation. University of Northumbria at Newcastle.

[6] AWAN, M. S., L. C. HORWATH, S. S. MUHAMMAD, E. LEITGEB, F. NADEEM and M. S. KHAN. Characterization of Fog and Snow Attenuations for Free-Space Optical Propagation. *Journal of Comumunications*. 2009, vol. 4, no. 8, pp. 533–545. ISSN 1796-2021, DOI: 10.4304/jcm.4.8.533-545.

[7] MOHAMMED, N. A., A. S. EL-WAKEEL and M. H. ALY. Performance Evaluation of FSO Link Under NRZ-RZ Line Codes, Different Weather Conditions and Receiver Types in the Presence of Pointing Errors. *The Open Electrical & Electronic Engineering Journal*. 2014, vol. 6, iss. 1, pp. 28–35. DOI: 10.1145/1509315.1509370.

[8] LIU, N., W. D. ZHONG, Y. HE, K. H. HENG a T. H. CHENG. Comparison of NRZ and RZ modulations in laser intersatellite communication systems. In: *Proceedings of the 2008 International Conference on Advanced Infocomm Technology - ICAIT '08*. New York: ACM, 2008, pp. 1–4. ISBN 978-1-60558-088-3. DOI: 10.1145/1509315.1509370.

[9] CHAND, N., J. LORIZ, A. J. HUNTON and B. M. ETESON. Performance comparison of NRZ and RZ modulations with and without forward error corrections for free-space optical communication. In: *Proceedings of SPIE, Free-Space Laser Communications V (58920U)*. London: SPIE, 2005, pp. 1–8. ISBN 9780819458971. DOI: 10.1117/12.621393.

[10] DAVID, A. and P. E. JOHNSON. Handbook of Optical Through the Air Communications. In: *Imagineering E-Zine* [online]. 2009. Available at: `http://www.imagineeringezine.com/ttaoc-pdf/OTTAC-Handbook.PDF`.

[11] LAMBERT, S. G. and W. L.CASEY. *Laser Communications in Space*. London: Artech House, 1994. ISBN 978-0890067222.

[12] AWAN, M. S. *Study of the Statistical-Dinamical Channel Modeling of Outdoor Optical Wireless Links*. Graz, 2010. Dissertation. Graz university of Technology.

[13] HRANILOVIC, S. *Wireless Optical Communication Systems*. New York: Springer, 2005, xii, pp. 196. ISBN 03-872-2785-7.

[14] RAMIREZ-INIGUEZ, R., S. M. IDRUS and Z. SUN. *Optical Wireless Communications: IR for Wireless Connectivity*. Boca Raton: CRC Press, 2008. ISBN 08-493-7209-7.

[15] BARUA, B. and S. P. MAJUMDER. Free Space Optical Communication with OOK and BPSK Modulation Under Different Turbulent Condition. In: *International Conference on Informatics, Electronics and Vision (ICIEV)*. Dhaka: IEEE, 2013, pp. 1–5. ISBN 978-1-4799-0397-9. DOI: 10.1109/ICIEV.2013.6572720.

[16] POPOOLA, W. O. and Z. GHASSEMLOOY. BPSK Subcarrier Intensity Modulated Free-Space Optical Communications in Atmospheric Turbulence. *Journal of Lightwave Technology*. 2009, vol. 27, iss. 8, pp. 967–973. ISSN 0733-8724. DOI: 10.1109/JLT.2008.2004950.

[17] TANG, X., S. RAJBHANDARI, W. O. POPOOLA, Z. GHASSEMLOOY, E. LEITGEB, S. S. MUHAMMAD and G. KANDUS. Performance of BPSK Subcarrier Intensity Modulation Free-Space Optical Communications using a Log-normal Atmospheric Turbulence Model. In: *Symposium on Photonics and Optoelectronics*. Chengdu: IEEE, 2010, pp. 1–4. ISBN 978-1-4244-4963-7. DOI: 10.1109/sopo.2010.5504014.

[18] KIM, I. I. Wireless Optical Transmission of Fast Ethernet, FDDI, ATM, and ESCON Protocol Data Using the TerraLink Laser Communication System. *Optical Engineering*. 1998, vol. 37, iss. 12, pp. 3143–3155. ISSN 0091-3286. DOI: 10.1117/1.601981.

[19] CAPLAN, D. O., B. S. ROBINSON, M. L. STEVENS, D. M. BOROSON and S. A. HAMILTON. High-rate Photon-efficient Laser Communications with Near Single Photon/bit Receiver Sensitivities. In: *Optical Fiber Communication Conference, 2006 and the 2006 National Fiber Optic Engineers Conference*. Lexington: IEEE, 2006, pp. 1–3. ISBN 1-55752-803-9. DOI: 10.1109/OFC.2006.215394.

[20] ZALUD, V., S. M. IDRUS and Z. SUN. *Moderni radioelektronika: IR for wireless connectivity*. 1st ed. Prague: BEN–Technical literature, 2000. ISBN 80-860-5647-3.

[21] VANDERKA, A. *Study of the Atmospheric Environment Effects on the Modulation Type in Free Space Optic*. Ostrava, 2013. Diploma Thesis. VSB–Technical University of Ostrava.

[22] KVICALA, R. Universal Optical Transmitter. *Elektrorevue*. 2006, vol. 6, iss. 1, pp. 1–8. ISSN 1213-1539. Available at: `http://www.elektrorevue.cz/clanky/05006/index.html#2`.

[23] DOLECEK, J. *Modern Literature of Electronics*. Prague: BEN–Technical literature, 2005. ISBN 80-730-0184-5.

[24] ELGANIMI, T. Y. Studying the BER Performance, Power and Bandwidth Efficiency for FSO Communication Systems Under Various Modulation Schemes. *IEEE Jordan Conference on Applied Electrical Engineering and Computing Technologies (AEECT). IEEE*. Amman: IEEE, 2013, pp. 1–6. ISBN 978-1-4799-2305-2. DOI: 10.1109/AEECT.2013.6716426.

[25] WILFERT, O. and Z. KOLKA. Statistical Model of Free-Space Optical Data Link. In: *Proceedings of SPIE: Free-Space Laser Communications IV (5550)*. Denver: SPIE, 2004, pp. 203–213. ISBN 9780819454881. DOI: 10.1117/12.558697.

[26] GHASSEMLOOY, Z., W. O. POPOOLA and E. LEITGEB. Free-Space Optical Communication Using Subcarrier Modulation in Gamma-Gamma Atmospheric Turbulence. In: *9th International Conference on Transparent Optical Networks*. Rome: IEEE, 2007, pp. 156–160. ISBN 1-4244-1249-8. DOI: 10.1109/icton.2007.4296269.

[27] SONG, X. YANG, F. and JULIAN CHENG. Subcarrier BPSK modulated FSO communications with pointing errors. In: *IEEE Wireless Communications and Networking Conference (WCNC)*. Shanghai: IEEE, 2013, pp. 4261–4265. ISBN 978-1-4673-5939-9. DOI: 10.1109/WCNC.2013.6555262.

[28] Wideband, Low-Noise, Voltage-Feedback Operational Amplifier: OPA846. In: *Texas Instruments* [online]. 2002: `http://www.ti.com/lit/ds/symlink/opa846.pdf`.

[29] Wideband, Ultra-Low Noise, Voltage-Feedback Operational Amplifier with Shutdown: OPA847. In: *Texas Instruments* [online]. 2002. Available at: `http://www.ti.com/lit/ds/symlink/opa847.pdf`.

[30] LM7171 Very High Speed, High Output Current, Voltage Feedback Amplifier. In: *Texas Instruments* [online]. 2014. Available at: `http://www.ti.com/lit/ds/symlink/lm7171.pdf`.

[31] PEREZ, J., Z. GHASSEMLOOY, S. RAJBHANDARI, M. IJAZ and H. Le MINH. Ethernet FSO Communications Link Performance Study Under and Controlled Fog Environment. *IEEE Communications Letters*. 2012, vol. 16, iss. 3, pp. 408–410. ISSN 1089-7798. DOI: 10.1109/lcomm.2012.012412.112072.

About Authors

Ales VANDERKA was born in in 1988 in Vitkov. He finished M.Sc. study at the VSB–Technical Uni-

versity of Ostrava, Faculty of Electrical Engineering and Computer Science, Department of Telecommunications in 2013. In present time he is Ph.D. student at VSB–Technical University of Ostrava. He focuses on optical technologies and especially Free Space Optic.

Lukas HAJEK was born in 1989 in Bohumin. In 2013 he finished M.Sc. study at VSB–Technical University of Ostrava, Faculty of Electrical Engineering and Computer Science, Department of Telecommunications. In present time he is Ph.D. student at VSB–Technical University of Ostrava. His interests are Free Space Optics and aging of optical communication components.

Jan LATAL was born in Prostejov. In 2006 he was awarded his B.Sc. degree at VSB–Technical University of Ostrava, Faculty of Electrical Engineering and Computer Science, Department of Electronics and Telecommunications. He was awarded his M.Sc. degree at VSB–Technical University of Ostrava, Faculty of Electrical Engineering and Computer Science, Department of Telecommunications in 2008. He is currently Ph.D. student, and he works in the field of Wireless Optical Communications, Optical Communications and Distributed Temperature Sensing Systems. He is a member of SPIE.

Jan VITASEK was born in Opava. In 2009 he finished M.Sc. study at Brno University of Technology, Faculty of Electrical Engineering and Communication. In 2014 he finished Ph.D. study at Department of Telecommunications, VSB–Technical University of Ostrava. His interests are Free Space Optics, indoor Free Space Optics networks and visible light communication. He is a member of SPIE. He is engaged in project dealing with VLC.

Petr KOUDELKA was born in 1984 in Prostejov. In 2006 he completed his Bachelor studies at VSB–Technical University of Ostrava, Faculty of Electrical Engineering and Computer Science, Department of Electronics and Telecommunications. Two years later he got his M.Sc. degree in the field of optoelectronics. At present he is in his Ph.D. studies and he is interested in VLC (Visible Light Communication), Distributed Temperature Sensing systems and optical technologies Passive Optical Networks.